

Applicability of in situ imaging to investigate copepod DVM patterns and morphology

Alex Barth Joshua Stone

10 Feb 2023

1 Introduction


Diel vertical migration (DVM) is a wide spread phenomena with large consequences in ocean ecosystems. DVM is the process of pelagic organisms moving up and down in the water column on a daily basis, often over a distance of dozens to hundreds of meters (Bianchi and Mislan 2016). This large-scale event occurs across a range of taxonomic and functional groups, from plankton to fish (Brierley 2014). However, DVM is particularly notable in zooplankton communities, whose daily migrations contribute substantially to biogeochemical cycles (Steinberg and Landry 2017; Archibald et al. 2019; Siegel et al. 2023). Zooplankton communities, largely dominated by copepods (Turner 2004), will feed in surface layers of the ocean then migrate deeper into the mesopelagic. Through excretion and respiration, copepods actively transport carbon to depth rather than sinking fluxes. Beyond carbon sequestration, Kelly et al. (2019) described zooplankton DVM is a major component of mesopelagic food webs, where productivity is often unfeasible. However, DVM can be extremely variable over temporal and spatial



scales (Bianchi and Mislan 2016; Gastauer et al. 2022). Thus it is important to understand the adaptive and environmental drivers of this behavior.

DVM has long been studied in marine systems (Bandara et al. 2021). The predominant pattern for zooplankton DVM is the movement from deep waters at daytime to shallower waters at night (Hays 2003; Bianchi and Mislan 2016). However, reverse migrations have been documented (Ohman 1990). There have been several hypotheses as to the proximate and ultimate drivers of DVM. However, when evaluating the adaptive benefits of DVM, there is substantial support [the](#) predator-avoidance hypothesis (Bandara et al. 2021). This hypothesis suggests that zooplankton evacuate the sunlit surface to evade visual predators. Then copepods ascend at night to graze on phytoplankton, who are restricted to the euphotic zone for productivity. The massive migration undertaken by these copepods is energetically expensive [\(](#)Maas et al. 2018). Therefore, the predator-avoidance hypothesis suggests that DVM is a result of an individual's visual [risk](#) exceeding the costs of its migration. However, a copepod's visual risk to a planktivorous fish varies greatly based on individual morphological features and surrounding environmental conditions (Aksnes and Utne 1997). Notably an individual copepod's size can increase visual detection risk. Several field-observations and simulation-based studies have suggested copepod size influences DVM magnitude (Hays et al. 1994; Aarflot et al. 2019; Pinti et al. 2019). This size dependent relationship however also varies across environmental conditions which influence light availability (Ohman and Romagnan 2016; Gastauer et al. 2022). At a global scale, ~~sun angle and consequentially seasonality~~ [also](#) have been shown to influence DVM magnitude (Bianchi and Mislan 2016). Given these observations about the

variability of visual detection, it is presumable that a copepod's color and transparency will influence DVM. Hays et al. (1994) reported that pigmentation could explain DVM frequency once having accounted for size. However, fewer studies have investigated this at length. One barrier to better studying how copepod traits influence DVM behavior is the difficulty of sampling and accurately recording traits. Yet understanding how morphology and environmental conditions influence DVM is critical for predicting how DVM may vary over time or changing ocean conditions.


In situ imaging tools have great potential to address some of the barriers to describing copepod DVM. By directly observing a copepod in its natural state, new ecological insights into their behavior and traits can be resolved (Ohman 2019). For example, Whitmore and Ohman (2021) used an in situ imaging device to describe a clear relationship of copepod abundance with a particulate field rather than chlorophyll-a. Such findings are facilitated by the fact imagery data records the exact position of a copepod in the water column. Additionally, a copepod's true appearance can be described compared to net-collected organisms whose guts are often evacuated and subjected to pigmentation loss in preservatives. Some studies have noted a DVM signal with copepods using in situ imagery data (Pan et al. 2018; Whitmore and Ohman 2021). However, direct tests of DVM-related hypotheses with such data have not been investigated. One potential challenge is that in situ imaging devices have extremely low sampling volumes compared to nets (Lombard et al. 2019). This low sampling volume creates difficulty for accurate quantification of large particles, plankton in particular, who are often times scarce (Barth and Stone 2022; Bisson et al.). As such, many studies testing DVM-related

60 hypotheses are restricted to acoustic data [CITES]. Nonetheless  we use

61 In this study, we investigate the applicability of in-situ imaging data to test DVM-related
62 hypotheses. We aim to test two hypotheses. First, (H  Overall copepod morphology, including
63 size and transparency, will impact DVM behavior. It is predicted that copepods which are
64 more visually detectable, e.g. larger and darker, will have larger diel migrations. Second, (H 
65 DVM behavior will vary based on environmental conditions related to the risks and rewards
66 of occupying surface waters. Specifically, increased prey availability will increase a copepod's
67 likelihood to travel to surface waters, while increased light availability will force copepods to
68 deeper sections of the water column. To test these hypotheses we build on novel statistical
69 tools to describe morphology of objects sampled by in situ imaging (Vilgrain et al. 2021;
70 Trudnowska et al. 2021; Sonnet et al. 2022). Additionally we evaluate multiple approaches to
71 describing DVM using in situ imaging data and how to estimate the impact of environmental
72 factors on DVM behavior.

73 2 Methods

74 2.1 CTD profiles and UVP imaging of copepods

75 Data were collected aboard the R/V Atlantic Explorer in collaboration with the Bermuda
76 Atlantic Time-series Study (BATS) (Steinberg et al. 2001). In situ images of plankton were
77 acquired using an Underwater Vision Profiler (UVP5-D  , sn: 209, Hydroptic, (Picheral et
78 al. 2010)). The original sampling methodology and instrument specification followed details

described in (Barth and Stone 2022). A brief summary of new and relevant sampling methodology are described below. The UVP was attached to the CTD rosette aboard the R/V Atlantic Explorer. The UVP was equipped for monthly cruises into the Sargasso Sea from June 2019 - Aug 2019 and October 2020 - December 2021. A typical monthly cruise included 13 profiles with descents typically to 1200m. Full cast details are available in Supporting Information. Only profiles within the BATS region were included (Figure 1). Generally, as described in analyses below, it was assumed that profiles within the BATS region during a cruise sampled a similar water mass. While mesoscale features are known to drive variability in this region, there were no major variations within a cruise (Supplemental Figure 1). The CTD collected continuous environmental parameters on down-casts, including temperature (Dual SBE-03f, Sea Bird Scientific), conductivity (Dual SBE04, Sea Bird Scientific), dissolved oxygen (SBE43, Sea Bird Scientific) and fluorescence (Chelsea Instruments). Because the purpose of this study was to investigate day/night differences in copepod vertical distributions, it was important that there were day and night casts during each cruise. It would be ideal to investigate each profile, without pooling the entire region by cruise, however, the small sampling volume of the UVP and low abundance of plankton in this region create the need to pool or average profiles (Barth and Stone 2022). Profiles were assigned to be day or night based on locally calculated nautical dawn and nautical dusk times using the R package `suncalc` 0.5.1.

The UVP sampled during down-casts of all profiles at a rate of ~15Hz. The UVP records counts of small particles ($>184\mu\text{m}$ Equivalent Spherical Diameter, ESD) and images of large particles ($>600\mu\text{m}$ ESD). However, living particles are not reliably identifiable below 0.9 mm

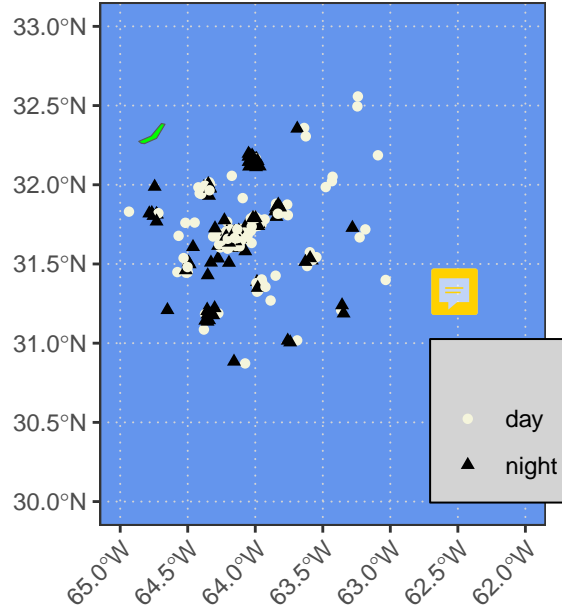


Figure 1: Figure 1. Map of CTD and UVP profiles used in the study. Day and night points from all cruises are shown. Bermuda is shown in green.

(Barth and Stone 2022). All recorded images were processed using Zooprocess (Gorsky et al. 2010), which provides several metrics related to size, grey value, and shape complexity. These features were then used to automatically sort images using the Ecotaxa application (Picheral et al.). While automatic classification increases the overall speed of identification (Irisson et al. 2022), all images were manually verified by the same trained taxonomist. In total, 294913 images were recorded. Of these, 85.2% were images of debris, marine-snow, or artefacts, while 14.8% were identified as living. In the present study, only copepods were investigated. The smallest observed and identified copepod was 0.940 mm ESD and the largest was 5.904 mm ESD. Across all casts, copepods were the most common observed organism at 58.7% of all identified, living particles. In total, there were 4151 individual copepods investigated in this

study.

2.2 Identification of morphogroups classification

To test the hypothesis of morphological influences on DVM magnitude, copepod images were classified into distinct morphological-groups (referred to as morphogroups). The UVP automatically measures and collects several morphologically relevant parameters. To create relevant groups of copepods, a dimension reduction and clustering approach was used. Similar methods have been successfully utilized to provide novel insights to marine snow (Trudnowska et al. 2021), copepod dynamics in the Arctic (Vilgrain et al. 2021), and temporal trends in phytoplankton communities (Sonnet et al. 2022). First, 18 parameters were selected to be included in a Principle Components Analysis (PCA) which represent major copepod morphological features following (Vilgrain et al. 2021). Parameters can be described as relating to size (e.g. major axis, feret diameter, ESD), grey intensity (e.g. mean grey value), shape (e.g. elongation, symmetry), and shape complexity (e.g. fractal dimension, perimeter/feret). All parameters and model structure are available in Supporting Information. The PCA was weighted by the volume sampled in a 1-m depth bin for each observation included in the model. This approach provides a correction for the UVP's variable descent speed which can cause duplicate imaging of individuals. While this phenomena has a minor impact on overall results (Barth and Stone 2022), we used the weighted approach to assure that no individual features were over represented. An unweighted PCA did not produce substantially different results, which supports the notion that duplicate images are a minor phenomena. All morpho-

logical descriptors were scaled and centered prior to inclusion in the analysis. The model was constructed using the R package **FactoMineR** 2.7. Principle components were deemed to be significant if their eigenvalues were greater than 1. This approach yielded 4 PCs which describe 87.3% of the total variation in morphological parameters, with 34.5% and 26.5% in the first two components respectively. This four principle component space provides a “morphospace” to characterize copepods.

Then to classify distinct morphogroups, a k-means clustering algorithm was used on the principle components (Trudnowska et al. 2021). While, there were 4 significant PCs, only the first two were used in the k-means clustering. Similar to Vilgrain et al. (2021), the third axis could be described by the orientation of the copepod to the camera and the fourth axis could be used to describe appendage visibility. Presumably, ~~the both~~ these factors would be random with respect to the depth at which a copepod was found. Possibly, appendage visibility could have a relationship with feeding activity, yet when included in the cluster analysis, no group clearly separated along this axis. Thus for simplicity, only the first two axes were included in the k-means clustering algorithm. To select the optimal number of clusters, clusters were added until the addition of a new cluster would not produce an increase the overall explanatory power ($\frac{WithinSS}{TotalSS}$) by more than 10%. This process identified four distinct morphogroups. The k-means clustering algorithm was ran with 1000 random starts. All code for the PCA and k-means models can be found in the supporting information. Additional model diagnostics are available in Supporting Information 2.

2.3 Investigating copepod vertical structure

Copepods in this system are well documented to undergo DVM (Steinberg et al. 2000; Schnetzer and Steinberg 2002; Maas et al. 2018). However, direct measurements of DVM using in situ imaging are not common. Thus, there are not established methods to describe DVM differences between groups or relation to environmental parameters. Here, we use and evaluate several approaches to specifically test DVM variation between morphogroup and in response to environmental factors. These include both classic and novel methods.

2.3.1 Vertical distribution of copepods

To visualize copepod vertical structure across morphogroups, the concentration of each morphogroup was calculated in 20m depth-bins for each UVP profile.

These binned-profiles were then averaged together based on time of day. This average-cast approach is useful as it provides a general pattern with information as to the variability between casts. Then to better estimate the day-night differences within each morphogroup, a proportional difference was calculated in each depth bin. A morphogroup's proportional difference was defined for each i depth bin as $Prop\ Diff_i = \frac{Night_i - Day_i}{\sum_i^N Night_i + Day_i}$, where $Night_i$ and Day_i are the average concentrations in that bin. By scaling each bin's diel difference by the total morphogroup concentration, it is possible to compare the profiles of proportional difference without the influence of difference in total concentration between morphogroups or depth bins. The proportional difference profile then was used to select a maximum depth (600m) to include


for the weighted mean depth calculations.

2.3.2 Weighted mean depth variability


Weighted mean depth (WMD) is a common metric to describe vertical structure and DVM in zooplankton *CITE*. However, with in-situ imagery, this approach presents a few challenges. WMD cannot be calculated individually for each profile then averaged because each profile had a different descent depth. Similarly, profiles had different sampling efforts throughout the water column. So to calculate the WMD for each morphogroup and each time of day, all 20-m binned concentrations from (0,20] to (580, 600], were pooled together. Then a bootstrap method was used to describe the variability in profiles and vertical structure. A traditional bootstrap approach would not work however, because there were more instances of shallow depth bins (as not all casts went as deep) so it would bias estimates. To correct for this, we define a bin-constrained approach to estimate a bootstrapped WMD^* .

$$WMD_{mg,tod}^* = \sum_i^{N=60} \frac{d_i(conc_{i,mg,tod}^*)}{\sum_i^{N=60} conc_{i,mg,tod}^*}$$

For each morphogroup (mg) and each time of day (tod), the WMD^* was calculated by randomly sampling a concentration from the pooled distribution of concentrations for each depth bin i . This was done for all 60 depth bins above 600m. The concentration was then multiplied by the midpoint of the depth bin and divided by the sum of all randomly sampled concentrations. This process was iterated 999 times to create a distribution of WMD^* for

186 each morphogroup and time of day. For each iteration, the concentrations for a depth bin
187 were randomly drawn with replacement for the next iteration. This approach effectively sim-
188 ulates multiple even profiles over the entire study region using the data from existing profiles.
189 Then a bootstrapped mean and 95% confidence interval were calculated from that distribu-
190 tion of *WMD**. The ~~the~~ bootstrapped confidence interval can then be interpreted as  ~~water~~ for
191 both variability between UVP profiles and the overall spread of the zooplankton in the water
192 column. Consequentially, it can be said a morphogroup exhibits a clear/significant signal of
193 DVM if the confidence intervals are non-overlapping between day and night.

194 2.3.3 Occupancy modelling of vertical structure

195 While the bootstrapped WMD depth is useful for investigating broad-scale DVM patterns
196 across the whole data set, it is ~~a~~ less effective when separating the data set into specific months
197 and seasons. Again issues arise with the compounding effect of the UVP's low sampling volume
198 and the rarity of organisms in this oligotrophic system. As described in detail by Bisson et al.,
199 when sampling volumes are low  estimating the theoretical probability of correctly estimating
200 particle concentration greatly decreases. In the present system, when specific morphogroups
201 are quite rare for a given season or month, the estimate of concentration greatly depends on
202 the presence/absence of that taxa in a depth bin and is not reliable as a result. To investigate
203 the environmental impact on DVM, the vertical structure needs to be compared across cruises,
204 or at least seasons. Therefore, using the WMD approach is not applicable because the split
205 data sets would be too small.

206 Here, we investigate the novel application of site-occupancy models to this data set. Site-
 207 occupancy models are a hierarchical-model popularized in biogeography and conservation bi-
 208 ology Kéry and Schmidt (2008). Often used with presence/absence data, the fundamental
 209 concept behind site-occupancy models is that the process of observing an organism at a given
 210 location is a function of the probability the organisms is there (occupancy/occurrence prob-
 211 ability, ψ) and the probability of detecting the organism given the sampling methodology
 212 (detection probability, p). These are an attractive class of models to apply to zooplankton
 213 in-situ imaging data because the detection probability is likely influenced by the sampling
 214 volume of the instrument while the occupancy is likely influenced by environmental/biological
 215 factors. To construct a site-occupancy model which estimates detection probability, replicate
 216 “surveys” must be done to each “site”. For our data set, we define a “site” as a depth-bin
 217 on a particular cruise and a “survey” as a single UVP profile on that cruise. Conceptually
 218 this assumption is similar to pooling-casts together over a study area. To first validate the
 219 application of this model, we constructed a simple model using the presence/absence of all
 220 copepods (regardless of morphogroup).

$$Y_{ij,db,tod} \sim \text{Bernoulli}(p_{ij,tod} * z_{i,db,tod})$$

$$z_{i,db,tod} \sim \text{Bernoulli}(\psi_{db,tod})$$

$$\text{logit}(p_{ij,tod}) \sim a_0 + a_{vs,tod} * vs_{ij}$$

223 In this model, the event of observing a copepod at site i during survey j , for each depth bin db

224 and time of day tod , is a function of the observation process which is modeled by a Bernoulli
 225 process. The observation process occurs with the probability of the product of the detection
 226 probability, $p_{ij,tod}$, and the occupancy, $z_{i,db,tod}$. This model was ran for each depth-bin (20m
 227 intervals from 0-1200m) and each time of day (day or night). The occupancy (ψ), was assumed
 228 to be a unique, independent probability for each depth bin while the detection probability was
 229 modelling using a logistic regression to include the effect of volume sampled ($\alpha_{vs,tod}$). If the
 230 site occupancy model is effective in this system, it would be expected that there would be
 231 a positive effect of volume sampled on the detection probability. The models were ran three
 232 separate times, to estimate detection probability differences between the epipelagic (0-200m),
 233 upper mesopelagic (200-600m), and lower mesopelagic (600-1200m). Detection probability
 234 was likely to differ between these regions due to differences in UVP descent speed and thus
 235 sampling volume through the water column as described in (Barth and Stone 2022).

236 Following the general all copepod model, we repeated the model yet separating out the different
 237 morphogroups. This allowed the test of the method to describe DVM. If effective, it would
 238 be expected there to be a difference in occupancy between daytime and nighttime in regions
 239 where migration is occurring (near-surface to upper mesopelagic). This additionally provides
 240 another method to test the hypothesis (H1) that morphology will increase DVM behavior,
 241 as it would predict the difference in day/night occupancy would be larger for more visually
 242 conspicuous morphogroups.

243 Finally, to evaluate the hypothesis that environmental conditions would influence DVM behav-
 244 ior, a site-occupancy model was constructed with included environmental parameters into the

biological process for occupancy. Several metrics were selected to be included in the model. Two metrics corresponding to light availability were included, photosynthetically active radiation (PAR) and the diffuse attenuation coefficient ($\frac{1}{k_{490}}$). Ohman and Romagnan (2016) described a clear relationship between increasing $\frac{1}{k_{490}}$, or deeper light penetration into the water column, and increased DVM amplitude. As such, in the present system, it was predicted that increases in PAR and $\frac{1}{k_{490}}$ would have a negative effect on daytime occupancy in depth bins near the surface. PAR and $\frac{1}{k_{490}}$ were both obtained from the Aqua MODIS sensor (NASA Goddard Space Flight Center, Ocean Ecology Laboratory, Ocean Biology Processing Group 2014) in 4km resolution in a grid encompassing the entire study area (Figure 1). Satellite data were collected with daily resolution yet averaged together over a cruise period because they were being modeled as “site” covariates. Metrics related to food availability were included as well. The depth of the deep chlorophyll-a maximum (\$DCM_d\$) was included with the prediction that a deeper DCM_d would have a positive effect on deeper depth bin occupancy and a negative effect on shallower depth bin occupancy. This logic suggests that copepods are not likely to travel to the surface if there is not food available there. The DCM_d was calculated from CTD profiles concurrent with the UVP then averaged together over the course of a cruise as a site covariate. CTD data were accessed from (<http://batsftp.bios.edu/BATS/ctd/>) using the R package `batsFtpReadR` 0.1.0 (<https://github.com/TheAlexBarth/batsFtpReadR>). Finally the particle concentration $<450\mu\text{m}$ was included as it can be a useful representative of the zooplankton prey field (Whitmore and Ohman 2021; Gastauer et al. 2022). Here, we use the integrated epipelagic ($<250\text{m}$) prey field with the prediction that a decrease in epipelagic food would have a negative impact on occupancy in that region of the water column. All par-

267 ticle data were recorded with the UVP and the integrated epipelagic prey field was averaged
 268 across all casts on a cruise as a site covariate.

269 The full environmental model can largely follows the general site-occupancy model described
 270 above. However, in this model, the biological process that a site i would follow the occupancy,
 271 or occurrence probability as modeled by a logistic regression. This was conducted with distinct
 272 intercepts (separate models) for each time of day, depth bin, and morphogroup.

$$z_{i,db,tod,mg} \sim \text{Binomial}(\psi_{i,db,tod,mg})$$

273

$$\begin{aligned} \text{logit}(\psi_{i,db,tod,mg}) \sim & \beta_{0_{db,tod,mg}} + \beta_{dcm_d_{db,tod,mg}} * dcm_d_i + \beta_{prey_{db,tod,mg}} * prey_i \\ & + \beta_{par_{db,tod,mg}} * par_i + \beta_{\frac{1}{k_{490\ db,tod,mg}}} * \frac{1}{k_{490\ db,tod,mg}} \end{aligned}$$

274 Thus there was a separate effect for each parameter β on a depth bin (db), time of day (tod),
 275 and morphogroup (mg). This allows for the investigation of how the posterior credible interval
 276 for the slope of each effect changes with depth.

277 All site-occupancy models follow a Bayesian hierarchical structure. These models were sim-
 278 ulated using JAGS ver 4.3.1 using the R package `jagsUI` 1.5.2. All parameters were given
 279 vague priors. For fixed probabilities (α_0 , ψ in the general model, β_0), a Beta(1,1) prior
 280 was used. For all slope parameters (α_{vs} , all β 's), a weak normal ($\mu = 0$, $\sigma = 1/10$) was used.
 281 The MCMC algorithm was ran with three chains for 10,000 iterations. Chains were thinned
 282 at a rate of 2. All data used to inform slope parameters were standardized prior to inclusion
 283 to reduce autocorrelation.

2.4 Data availability

All data and code are made available via (https://github.com/TheAlexBarth/DVM_Migration-Morphology). All supplemental figures, tables, and analyses are hosted on a public static site (https://thealexbarth.github.io/DVM_Migration_Morphology). This content is also available in the Supporting Information.

3 Results

3.1 Morphogroup classification

The PCA revealed four major ~~axis~~ of variability (Figure 2). The first axis (PC1, 34.23% of variability) was largely explained by along a gradient of increasing values related to size, such as perimeter (loading score = 0.927) and feret diameter (loading score = 0.910).

The second axis (PC2, 27.24% of variability) can be interpreted primarily by a spectrum of transparent to dark/shaded individuals. PC2 was largely anticorrelated with mean grey value (higher values indicate a more transparent individual) (loading score = -0.920). As noted in the methods, PC3 and PC4 were both related to the orientation of the copepod and the appendage visibility respectively (Supplemental 3). As a result, these axis were not included in k-means clustering analysis.

The k-means clustering analysis yielded 4 morphogroups which represent over 64% of the total variation in the two-component morphospace (Figure 2). Morphogroup 1 primarily includes

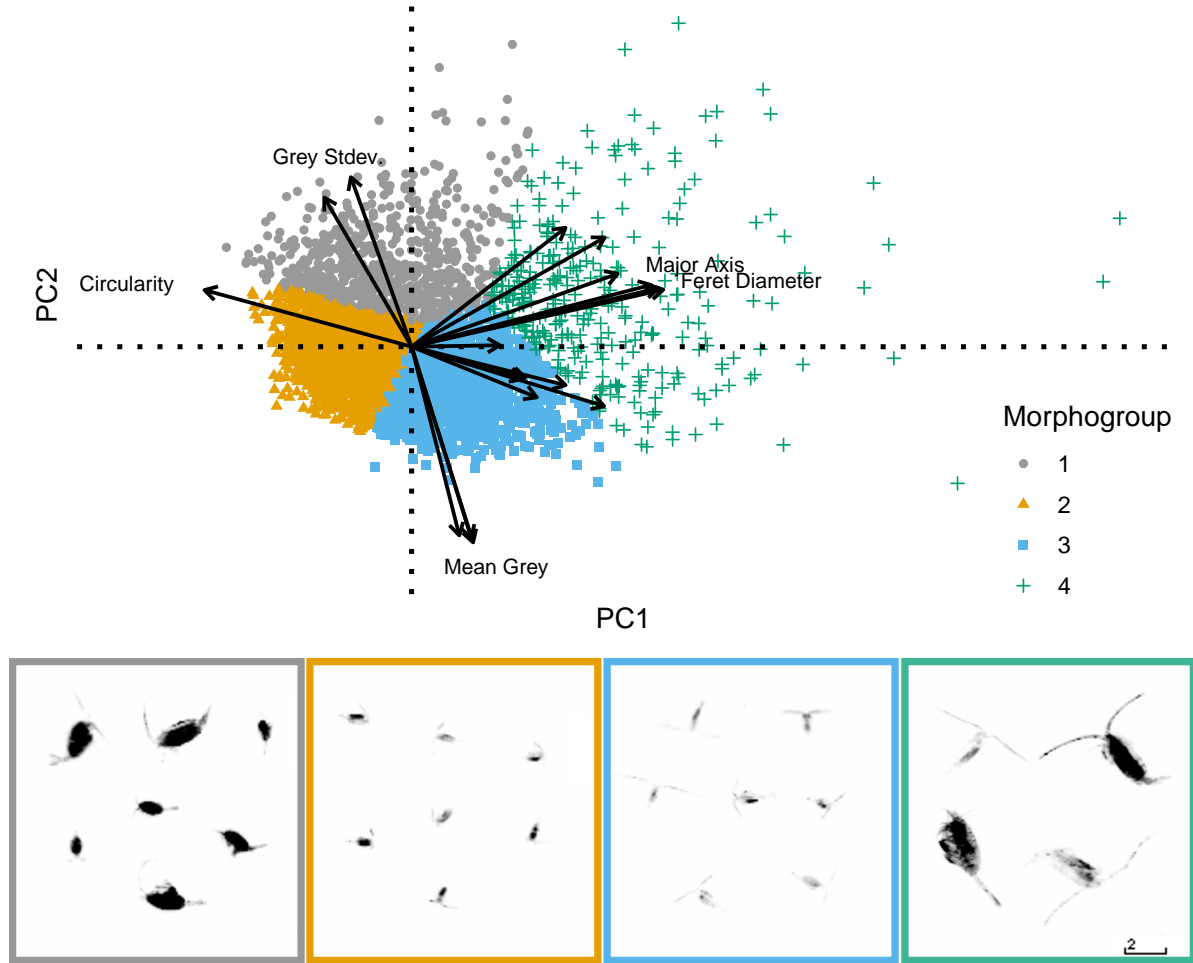


Figure 2: Morphogroups shown in the 2-component morphospace. PC1 represents 34.23% of total variability, PC2 represents 27.24%. Representative images from morphogroups 1-4 as identified by k-means clustering are shown in numerical order at bottom of the plot. Colored borders correspond to morphospace. 2mm scale bar is present in the bottom right.

small-to-medium, dark individuals with moderate PC1 scores and high PC2 scores (Figure 2, Figure 3B,D). Morphogroup 2 is best described by the smallest copepods, with low values on PC1 (Figure 2, Figure 3A,C). Morphogroup 3 is associated with moderate-to-big values of PC1 and negative values of PC2. Thus, morphogroup 3 largely contains more transparent, medium-to-large copepods (Figure 2, 3A,D). Finally, morphogroup 4 constituents are the largest copepods, spanning a wide range of shade values (Figure 2, Figure 3A,B,D).

To verify that the morphogroups were not arbitrary, a Dunn's pairwise comparison test was used with a Bonferroni correction. It was found that all groups were significantly different from one another ($p < 0.001$) along both principle components (Figure 3). To illustrate the difference along morphological parameters, morphogroups were plotted against mean feret diameter and mean grey value (Figure 3C,D). From these figures, it is evident that the morphogroups were different along morphologically specific parameters.

3.2 Morphogroup average concentration and vertical distribution

Across all cruises, the overall integrated (0-1200m) abundance of morphogroups followed a similar pattern. Abundance was higher during the spring-summer months and lowest during the fall and winter (Supplemental 4). Generally, the largest copepods (morphogroup 4) were less abundant in all cruises. The darker copepods (morphogroup 1) were also in lower abundance at some times of the year (Supplemental 4). The smaller copepods were more abundant (morphogroup 2), which is consistent with the notion this system is dominated by smaller individuals. Interestingly, morphogroup 3 tended to be more abundant than morphogroup

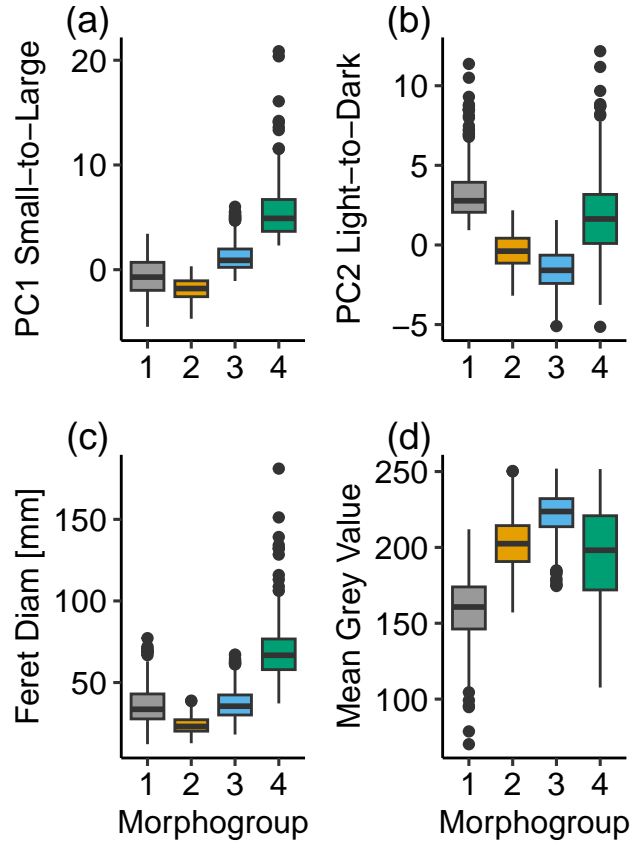


Figure 3: Distribution of morphogroups across (A) PC1, (B) PC2, (C) Feret Diameter, and (D) Mean Grey Value. Morphogroups were significantly different from another along PC1 and PC2 (Dunn test for multiple comparison, $p < 0.001$).

1 despite the presumption that morphogroup 3 consists of larger copepods. In some cruises, morphogroup 3 was the most abundant category (Supplemental 4).

By morphogroup, the overall patterns of average abundance are reflected in each average vertical profile (Figure 4A-D). Average abundance throughout the water column was higher in morphogroup 2 and morphogroup 3 then lowest in morphogroup 4. All morphogroups displayed a nighttime peak in average abundance near the lower epipelagic (100 - 200m) (Figure 4A-D). While all morphogroups had some concentration of copepods near the surface during the daytime, the proportional difference clearly showed nighttime abundances were higher, on average (Figure 4E-F). Additionally, copepod average abundances were low around ~~around~~ 200m-400m. Then from about 400m-600m, the average abundance of all morphogroups increased for daytime bins, but not nighttime. Below 600m, day/night differences were more stochastic, which is consistent with a reasonable exception for DVM to not extend this deep into the water column. It should be noted that the standard deviation in each depth bin's abundance is quite large (Figure 4A-D). The large variability both within and between cruises, likely drives the large variation in bin average abundance.

3.3 Weighted mean depth analysis

The bin-constrained bootstrap estimates of WMD for all morphogroups indicated a clear signal of DVM (Figure 5). The daytime 95% confidence intervals (CIs) were consistently non-overlapping and deeper than the nighttime 95% CIs (Figure 5). The mean, nighttime bootstrapped WMD for all four morphogroups was around 150-200m. This is consistent with

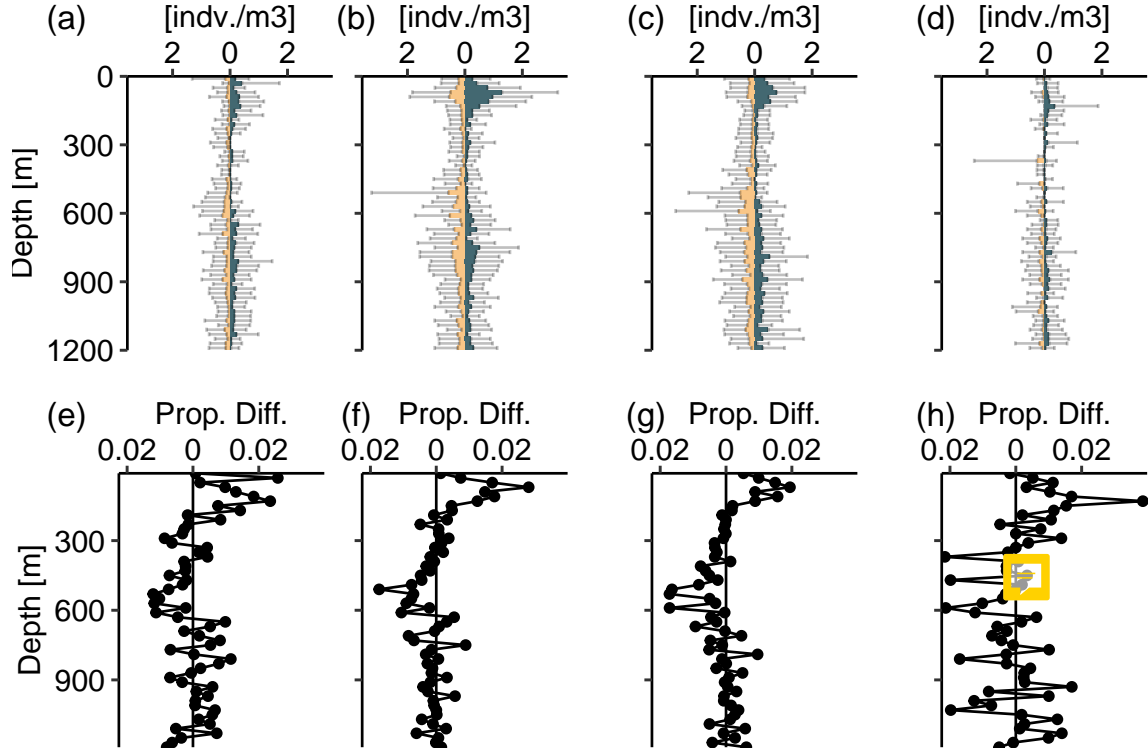


Figure 4: (A-D) Vertical profiles of average copepod concentration in 20m depth bins. Daytime concentrations are light-colored and shown left of the vertical axis, nighttime values are dark-colored and shown right of the vertical axis. (E-H) Proportional nighttime/daytime difference in 20m bins. A nighttime-dominated bin is right of the vertical axis, daytime-dominated left of the vertical axis. Vertically paired, panels correspond to an individual morphogroup; (A,E) Morphogroup 1, (B,F) Morphogroup 2, (C,G) Morphogroup 3, (D,H) Morphogroup 4

the peak in average abundance which occurred around 150m (Figure 4A-D). Generally, the daytime WMD 95% CIs were overlapping, spanning the upper mesopelagic. The exception to that observation is morphogroup 4, whose daytime WMD 95% CI is clearly shallower (non-overlapping) than the daytime WMD of morphogroups 2 and morphogroup 3. However, this difference, while statistically clear, may be an artifact of the sparseness of morphogroup 4 at depth (Figure 4D).

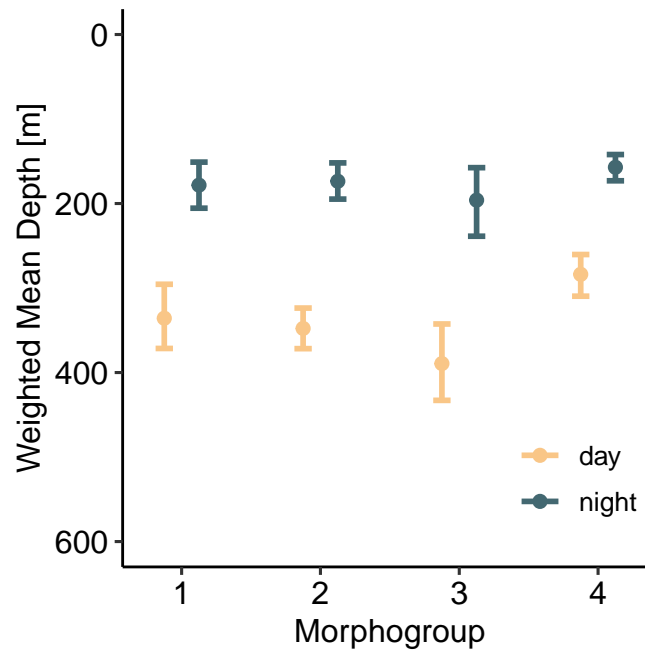


Figure 5: Weighted mean depth and 95% confidence intervals from bin-constrained bootstrapping approach. Values are displayed for each of the four morphogroups at both times of day.

3.4 Occupancy models

The first occupancy model using all copepods validated the occupancy model approach. The detection probability could be estimated from the posterior distributions for parameters in

351 the logistic regression (α_0 , α_{vs}). To visualize the detection probability (p), the posterior
 352 distributions for the parameters were multiplied across a range of possible sampling volumes
 353 (0-1,050 L). As expected, there was a clear relationship between increasing volume sampled
 354 and an increase in detection probability (Figure 6). This increase was present for all regions of
 355 the water column, however it was most prominent in the nighttime, shallower region (0-250m)
 356 (Figure 6A). Overall, detection probability was lower in the daytime shallow region and both
 357 times of day throughout mesopelagic. The average volume sampled in a 20-m wide depth
 358 bin was 526.2 L. While this corresponds to an over 50% detection probability in the nighttime
 359 upper-region, it corresponds to nearly 25% or below in all other times of day and water column
 360 regions. The higher detection probability in the nighttime epipelagic is likely a result of the
 361 increased concentration of copepods in that region of the water column (Figure 4A-D). The
 362 occupancy (ψ) estimates of all copepods showed a pattern consistent with their vertical average
 363 abundance profiles (Supplemental 5). ψ was high for both times of day in the epipelagic, with
 364 a decrease around 250m. The nighttime ψ also was reduced from about 400m-600m deep
 365 (Supplemental 5).

366 The general occupancy model for copepods by morphogroup revealed some clear trends consis-
 367 tent with DVM hypotheses. Generally, across all morphogroups, the credible intervals (95%
 368 high density interval of the posterior distribution for ψ) for copepod occupancy were very
 369 wide (Figure 7). The credible intervals often range from 25% to 100%. However, there is
 370 a notable increase in nighttime ψ for all morphogroups from 40m to 140m. For depth bins
 371 in that region, the mean posterior ψ ranged from 71% to 88%, indicating there is a high

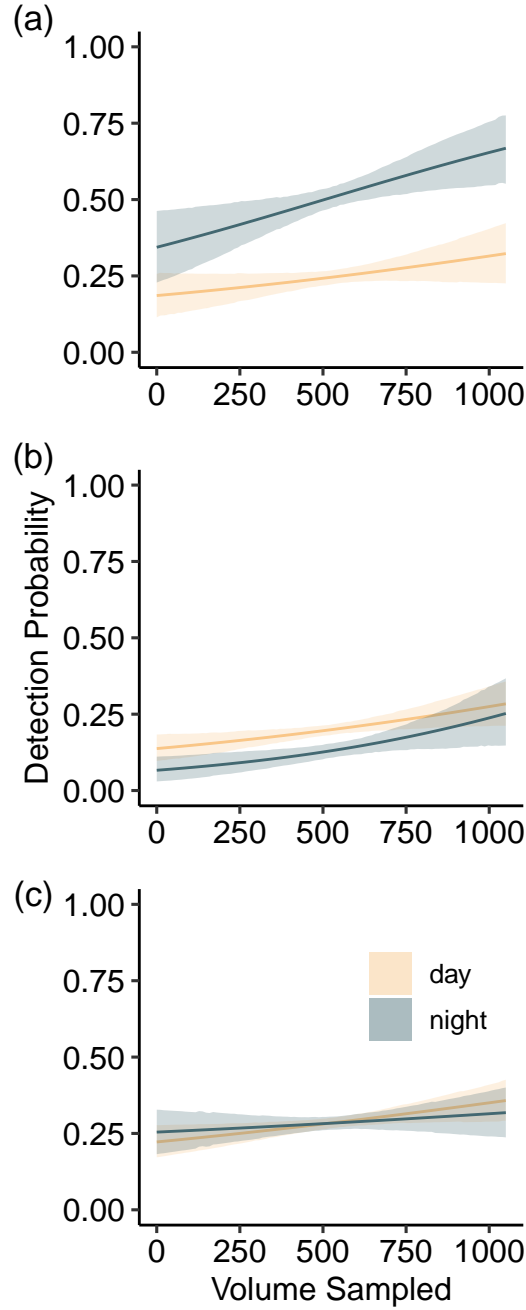


Figure 6: Detection probability across volume sampling range from the all-copepod occupancy model. The posterior distribution for model parameters were fit to an equally-spaced range of possible sampling volumes consistent with the UVP data. The model was run for three separate water column regions; (A) 0-250m, (B) 250-600m, and (c) 600-1200m. Regions were based on the variability of UVP descent speed and abundance of organisms. Separate intercepts for the model were also based on the time of day. Shaded region represents the 95% posterior credible interval

likelihood all morphogroups will be found in that region at night. There is lower daytime ψ over that same region, however this varies by morphogroup. Morphogroup 4 has a 54% mean posterior daytime ψ from 40m-140m (Figure 7D). This indicates a decreased likelihood of the larger, morphogroup 4 copepods in that area during daytime. All other morphogroups have higher posterior daytime ψ in the epipelagic. Generally, throughout the rest of the water column, the posterior estimates of ψ are high (Figure 6). Again there was a decline present around 225-300m, consistent with the average abundance profiles. Overall, morphogroup 4 had a wider credible interval around the posterior ψ estimate which is likely due to its rarity (Figure 4D, Figure 7D, Supplemental 4).

Finally to attempt to relate environmental impacts to DVM, the full environmental occupancy model was investigated. However, no discernible trends were found. There was no clear effect of any of the environmental parameters on the occurrence probability for any morphogroup, in any depth-bin, in any time of day. The posterior credible intervals for the slope of each parameter on the log odds of ψ typically ranged from -10 to 15. That change in log odds corresponds to an increase in occurrence probability of 0.00005% to 99% for each one unit increase of the environmental parameter. For all environmental parameters, the slope on the LOG ODDS(ψ) had a posterior mean near 0 (Supplemental 6).

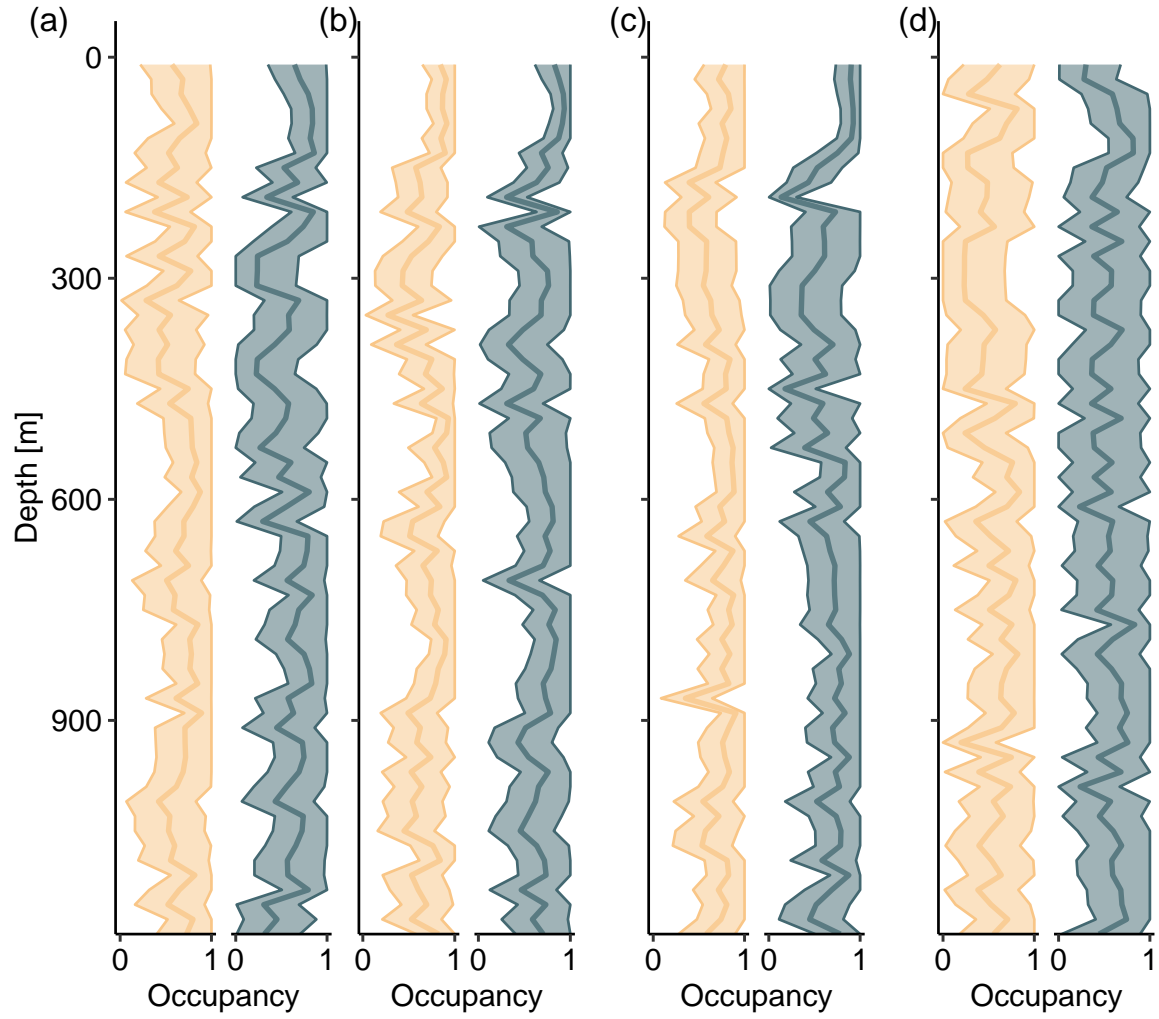


Figure 7: Occupancy (occurrence probability, ψ) of copepods from each morphogroup from basic occupancy model. Separate intercepts were fit for each time of day and each 20m depth bin. Values shown between depth bins are linearly interpolated which results in jagged points. Center line is the posterior mean occupancy while shaded region is the 95% posterior credible interval.

4 Discussion

4.1 Morphogroup delineation

This study builds on methods for describing morpho-spaces and morphogroups from several previous imaging studies (Vilgrain et al. 2021; Trudnowska et al. 2021; Sonnet et al. 2022). The PCA-defined morphospace with the present data aligns well with the prior applications of this approach. Interestingly, the morphospace defined with Arctic copepod images by Vilgrain et al. (2021) is extremely similar to the morphospace defined in this study using subtropic copepod images. The proportion of morphological variation explained by each of the four principle components are extremely close between these two studies. It is possible that this is an artifact of the similarity of input data. Given the UVP has a limited range of observable size classes (Picheral et al. 2010), only copepods above a certain size were fed into both PCAs. Nonetheless, it is striking that the two morphospaces are similar considering the vastly different community compositions between the Arctic ocean and subtropical gyres (Soviadan et al. 2022). It could be that copepod size variation can be reduced to the two major dimensions described in Vilgrain et al. (2021) and this study. To confirm this, work should be done applying this morphospace approach across instruments and ocean regions. Using phytoplankton images Sonnet et al. (2022) displayed how a morphospace can be used to compare community changes across time. Comparisons of copepod morphospaces across temporal and spatial scales may offer a useful metric for answering biogeographic and ecological questions.

The k-means clustering analysis to define morphogroups within the morphospace was first

done using marine snow imagery (Trudnowska et al. 2021). Using the copepod data set in this study, the k-means clustering successfully identified four distinct morphogroups. Although these morphogroups were significantly different along both principle components and varied along major morphological axis, the morphogroups did not lend themselves to a clear test of H1. Ideally to test the hypothesis that both size and color independently influence DVM, at least two groups would be similarly size yet vary in grey value. Regardless the designated morphogroups still lent themselves to meaningful investigation.

4.2 Description of DVM

Weighted mean depth is a classic approach used in describing DVM of zooplankton (Ohman et al. 2002; Aarflot et al. 2019). WMD was used with a net-collected dataset to characterize differences in DVM amplitude based on copepod size (Ohman and Romagnan 2016). With the in situ imagery data in this study, a modification of the WMD approach did successfully display a clear DVM signal. However, the results did not show a clear pattern of differences between morphogroups (Figure 5). This is likely a result of the sampling scheme which forced a binned bootstrapping approach. Had sampling volume been more consistent throughout the water column, it may have been feasible to calculate cast-specific WMD, then average values. This possibility may be approached with in situ imaging devices that can be deployed on gliders and floats (Ohman et al. 2019; Picheral et al. 2022). Due to the nature of our dataset however, the binned bootstrapping of the WMD created extremely large confidence intervals for some groups. These wide intervals are likely the result of large intercast variation.

429 The WMD analysis did suggest however, that the daytime depth of the largest copepods
430 (morphogroup 4) was shallower than smaller copepods (morphogroups 2 & 3). Given the
431 overwhelming support for large copepods occupying deeper waters during daytime (Ohman
432 and Romagnan 2016; Aarflot et al. 2019; Pinti et al. 2019), this contrary finding is probably
433 artificial. The overall abundance of morphogroup 4 was low, particularly at depth (Figure 4;
434 Supplemental 4). The lack of encounters with morphogroup 4 at deeper waters (200-600m)
435 likely resulted in the average daytime WMD not being pulled deeper as it was for the other
436 morphogroups who's overall abundances were higher. Overall, then WMD was not a suitable
437 analysis to test the hypothesis that morphology would influence DVM (H1). The misleading
438 result from this analysis is indicative of a problem of using WMD to describe the rare/poorly
439 sampled organisms from in situ imagery datasets. Additionally, because the WMD approach
440 required pooling of casts across multiple seasons, it reduced the ability to investigate seasonal
441 trends or environmental influences. A large draw of in situ imaging is the high frequency and
442 specificity of zooplankton observations, further suggesting that WMD is not a suitable analysis
443 for these types of data.

444 Alternatively, site-occupancy modelling suggested a successful tool for analysis of in situ
445 zooplankton images. Given that many observations of copepods in this dataset were pres-
446 ence/absence, site-occupancy models were a suitable fit. Additionally, treating copepods as
447 presence/absence circumvents challenges, although rare, that may arise from duplicate images
448 (Barth and Stone 2022). As to the characterization of DVM, site-occupancy models showed
449 promise. Notably, our morphogroup-specific analysis provided weak support for H1. Mor-

phogroup 4 had a larger DVM signal than the other morphogroups as noted by the decreased daytime ψ near the surface (Figure 7). However, contrary to the predictions of H1, there was no detectable effect of transparency/grey value on DVM signal. There are several possibilities for this results. First, it could be a limitation of lack of distinct morphogroups as described above. Specifically, morphogroup 4 spanned a wide range of grey values. Perhaps with a larger set of copepod images, this group could be split into two distinct groups based on grey-value. However, it could also be that grey-value as recorded by the UVP does not influence DVM in this system. Grey-value in UVP-imaged copepods can be indicative of many features beyond simply pigmentation, notably egg-sacs and gut contents (Vilgrain et al. 2021). Such characteristics vary much more between individuals and can have varied influences on DVM (PEARRE Jr. 2003). Additionally, while well documented, predator avoidance may not always be the primary selective pressure on copepod traits. For example, if the costs of migration are too large for some copepods, they will remain near the surface. However, these copepods then are exposed to UV light and may increase pigmentation to reduce UV damage. Likely the relationship between color and DVM is the result of a delicate balance of minimizing multiple ecological and biological risks (Hansson 2004; Hylander et al. 2014).

Finally, the environmental metrics included in an occupancy model were not able to distinguish any clear effect. This then does not provide any support to the hypothesis that environmental conditions would influence DVM (H2). This lack of result could be either a limitation of the model and sampling scheme or a reflection of real patterns. As discussed below, the “sites” were defined post-hoc as all casts, from each time of day, on a given cruise. While environmental

471 conditions were not extremely varied within cruises (Supplemental 2), treating a cruise as
 472 a single site may have been too broad and created too-high of encounter rates at a “site”
 473 to distinguish effects of environmental factors. However, it may also be that the recorded
 474 environmental conditions on in this study system did not vary enough to elicit differences
 475 in DVM behavior. For example, the diffuse attenuation coefficient ($\frac{1}{k_{490}}$) captured across
 476 all cruises ranged from 21.5m to 47.5m. ~~Competitively,~~ @ohman2016 measured copepods
 477 collected from environments that had the $\frac{1}{k_{490}}$ range from nearly 1m to over 30m, with a
 478 reduction in DVM amplitude not occurring until around 20m. Subtropical gyres have been
 479 described to have the largest DVM amplitudes with lower seasonal variation (Bianchi and
 480 Mislan 2016). Therefore, it is possible the lack of effect of environmental parameters in the
 481 analysis is reflective of actual conditions. It would be worthwhile for researchers to replicate
 482 this approach in different ocean ecosystems.

483 **4.3 Occupancy models: promises and limitations**

484 Site-occupancy models have been successfully utilized in terrestrial ecology and conservation
 485 biology (Royle 2006; Kéry 2010; MacKenzie et al. 2017). In marine systems, studies focusing
 486 on eDNA have utilized site-occupancy models (McClenaghan et al. 2020; Hinz et al. 2022).
 487 However, they have yet to be adapted specifically to pelagic plankton ecology. Here, we
 488 demonstrate a clear case for the application of site-occupancy models to in situ imagery data.
 489 First, using all copepods, regardless of morphogroup, the site-occupancy model revealed a
 490 clear relationship between volume sampled and detection probability. While the relationship

491 between sampling volume and detection is intuitive, this model confirms it and quantifies the
492 lack-of-detection. Additionally, the sampling volume detection relationship in the different
493 regions of the ocean suggests there is no visual avoidance of the CTD rosette by copepods
494 (Figure 6). Were there any visual-aided avoidance, it would be expected that the surface
495 waters would have lower detection than the mesopelagic, which was not the case.

496 The occupancy analyses in this study suggested extremely low detection probabilities (Figure
497 6). This is in part driven by the overall low abundances of copepods in this system (Figure
498 4, Supplemental 4). However, as previously discussed, it is also likely that the grouping of
499 casts to define “sites” was too broad. Within a site, there may have been copepods at a given
500 depth-bin yet some variations influencing occupancy variability between surveys (casts) would
501 suggest lower detection probabilities. Zooplankton populations are known to be extremely
502 patchy (Folt and Burns 1999). Such local-scale variability suggests that to fully utilize site-
503 occupancy models, sampling schemes ought to be carefully designed. Ideally replicate casts
504 in similar locations. While this may be challenging on ship-based operations, imaging devices
505 attached to autonomous gliders and floats can conduct several casts per day (Ohman et al.
506 2019; Gastauer et al. 2022; Picheral et al. 2022). Future studies should consider use of
507 site-occupancy modelling for the description of sparsely-imaged zooplankton.

5 Conclusions

Overall, this paper displays the possibility of hypothesis-driven investigation with in situ imaging. Minor support was found relating copepod size to DVM amplitude yet not with copepod transparency. Diel migration patterns across morphology remains an exciting question, size has clearly been shown to influence DVM behavior. However visual predation is a variable metric, related to the present community composition. Intuitively, transparency may influence visual risk however, our paper does not provide any support to this hypothesis. It may be that there are several contrasting pressures which influences copepod colors.

As in situ imaging progresses in the field of plankton ecology, new observations and datasets are rapidly growing. However, gaining insights from these data are limited by our ability to analyze the data with robust statistical methods. Here we demonstrate a promising approach for analyzing in situ imaging data despite the low-detection of mesozooplankton with common instruments.

References

- Aarflot, J. M., D. L. Aksnes, A. F. Opdal, H. R. Skjoldal, and Ø. Fiksen. 2019. Caught in broad daylight: Topographic constraints of zooplankton depth distributions. *Limnology and Oceanography* **64**: 849–859. doi:[10.1002/lno.11079](https://doi.org/10.1002/lno.11079)
- Aksnes, D. L., and A. C. W. Utne. 1997. A revised model of visual range in fish. *Sarsia* **82**: 137–147. doi:[10.1080/00364827.1997.10413647](https://doi.org/10.1080/00364827.1997.10413647)

- Archibald, K. M., D. A. Siegel, and S. C. Doney. 2019. Modeling the Impact of Zooplankton Diel Vertical Migration on the Carbon Export Flux of the Biological Pump. *Global Biogeochemical Cycles* **33**: 181–199. doi:[10.1029/2018GB005983](https://doi.org/10.1029/2018GB005983)
- Bandara, K., Ø. Varpe, L. Wijewardene, V. Tverberg, and K. Eiane. 2021. Two hundred years of zooplankton vertical migration research. *Biological Reviews* **96**: 1547–1589. doi:[10.1111/brv.12715](https://doi.org/10.1111/brv.12715)
- Barth, A., and J. Stone. 2022. [Comparison of an in situ imaging device and net-based method to study mesozooplankton communities in an oligotrophic system](#). *Frontiers in Marine Science* **9**.
- Bianchi, D., and K. a. S. Misan. 2016. Global patterns of diel vertical migration times and velocities from acoustic data. *Limnology and Oceanography* **61**: 353–364. doi:[10.1002/lno.10219](https://doi.org/10.1002/lno.10219)
- Bisson, K. M., R. Kiko, D. A. Siegel, L. Guidi, M. Picheral, E. Boss, and B. B. Cael. Sampling uncertainties of particle size distributions and derived fluxes. *Limnology and Oceanography: Methods* **n/a**. doi:[10.1002/lom3.10524](https://doi.org/10.1002/lom3.10524)
- Brierley, A. S. 2014. Diel vertical migration. *Current Biology* **24**: R1074–R1076. doi:[10.1016/j.cub.2014.08.054](https://doi.org/10.1016/j.cub.2014.08.054)
- Folt, C. L., and C. W. Burns. 1999. Biological drivers of zooplankton patchiness. *Trends in Ecology & Evolution* **14**: 300–305. doi:[10.1016/S0169-5347\(99\)01616-X](https://doi.org/10.1016/S0169-5347(99)01616-X)
- Gastauer, S., C. F. Nickels, and M. D. Ohman. 2022. Body size- and season-dependent diel vertical migration of mesozooplankton resolved acoustically in the San Diego Trough. *Limnology and Oceanography* **67**: 300–313. doi:[10.1002/lno.11993](https://doi.org/10.1002/lno.11993)

549 Gorsky, G., M. D. Ohman, M. Picheral, and others. 2010. Digital zooplankton image anal-
 550 ysis using the ZooScan integrated system. *Journal of Plankton Research* **32**: 285–303.
 551 doi:[10.1093/plankt/fbp124](https://doi.org/10.1093/plankt/fbp124)

552 Hansson, L.-A. 2004. Plasticity in Pigmentation Induced by Conflicting Threats from Preda-
 553 tion and Uv Radiation. *Ecology* **85**: 1005–1016. doi:[10.1890/02-0525](https://doi.org/10.1890/02-0525)

554 Hays, G. C. 2003. [A review of the adaptive significance and ecosystem consequences of zoo-](#)
 555 [plankton diel vertical migrations](#). Springer Netherlands. 163–170.

556 Hays, G. C., C. A. Proctor, A. W. G. John, and A. J. Warner. 1994. Interspecific differences
 557 in the diel vertical migration of marine copepods: The implications of size, color, and mor-
 558 phology. *Limnology and Oceanography* **39**: 1621–1629. doi:[10.4319/lo.1994.39.7.1621](https://doi.org/10.4319/lo.1994.39.7.1621)

559 Hinz, S., J. Coston-Guarini, M. Marnane, and J.-M. Guarini. 2022. Evaluating eDNA for
 560 Use within Marine Environmental Impact Assessments. *Journal of Marine Science and*
 561 *Engineering* **10**: 375. doi:[10.3390/jmse10030375](https://doi.org/10.3390/jmse10030375)

562 Hylander, S., J. C. Grenvald, and T. Kiørboe. 2014. Fitness costs and benefits of ultra-
 563 violet radiation exposure in marine pelagic copepods. *Functional Ecology* **28**: 149–158.
 564 doi:[10.1111/1365-2435.12159](https://doi.org/10.1111/1365-2435.12159)

565 Irisson, J.-O., S.-D. Ayata, D. Lindsay, L. Karp-Boss, and L. Stemmann. 2022. Machine
 566 learning for the study of plankton and marine snow from images. *Annual Review of Marine*
 567 *Science* **14**. doi:[10.1146/annurev-marine-041921-013023](https://doi.org/10.1146/annurev-marine-041921-013023)

568 Kelly, T. B., P. C. Davison, R. Goericke, M. R. Landry, M. D. Ohman, and M. R. Stukel. 2019.
 569 [The importance of mesozooplankton diel vertical migration for sustaining a mesopelagic](#)
 570 [food web](#). *Frontiers in Marine Science* **6**.

571 Kéry, M. 2010. Introduction to WinBUGS for ecologists: a Bayesian approach to regression,
572 ANOVA, mixed models and related analyses, 1st ed. Elsevier.

573 Kéry, M., and B. Schmidt. 2008. Imperfect detection and its consequences for monitoring for
574 conservation. *Community Ecology* **9**: 207–216. doi:[10.1556/ComEc.9.2008.2.10](https://doi.org/10.1556/ComEc.9.2008.2.10)

575 Lombard, F., E. Boss, A. M. Waite, and others. 2019. [Globally consistent quantitative](#)
576 [observations of planktonic ecosystems](#). *Frontiers in Marine Science* **6**.

577 Maas, A. E., L. Blanco-Bercial, A. Lo, A. M. Tarrant, and E. Timmins-Schiffman. 2018. Vari-
578 ations in copepod proteome and respiration rate in association with diel vertical migration
579 and circadian cycle. *The Biological Bulletin* **235**: 30–42. doi:[10.1086/699219](https://doi.org/10.1086/699219)

580 MacKenzie, D. I., J. D. Nichols, J. A. Royle, K. H. Pollock, L. L. Bailey, and J. E. Hines.
581 2017. *Occupancy Estimation and Modeling: Inferring Patterns and Dynamics of Species*
582 *Occurrence*, Elsevier.

583 McClenaghan, B., Z. G. Compson, and M. Hajibabaei. 2020. Validating metabarcoding-based
584 biodiversity assessments with multi-species occupancy models: A case study using coastal
585 marine eDNA. *PLOS ONE* **15**: e0224119. doi:[10.1371/journal.pone.0224119](https://doi.org/10.1371/journal.pone.0224119)

586 NASA Goddard Space Flight Center, Ocean Ecology Laboratory, Ocean Biology Processing
587 Group. 2014. MODIS-aqua ocean color data.

588 Ohman, M. D. 1990. The Demographic Benefits of Diel Vertical Migration by Zooplankton.
589 *Ecological Monographs* **60**: 257–281. doi:[10.2307/1943058](https://doi.org/10.2307/1943058)

590 Ohman, M. D. 2019. A sea of tentacles: optically discernible traits resolved from planktonic
591 organisms in situ H. Browman [ed.]. *ICES Journal of Marine Science* **76**: 1959–1972.
592 doi:[10.1093/icesjms/fsz184](https://doi.org/10.1093/icesjms/fsz184)

Ohman, M. D., R. E. Davis, J. T. Sherman, K. R. Grindley, B. M. Whitmore, C. F. Nickels, and
J. S. Ellen. 2019. Zooglider: An autonomous vehicle for optical and acoustic sensing of zoo-
plankton. *Limnology and Oceanography: Methods* **17**: 69–86. doi:[10.1002/lom3.10301](https://doi.org/10.1002/lom3.10301)

Ohman, M. D., and J.-B. Romagnan. 2016. Nonlinear effects of body size and optical at-
tenuation on Diel Vertical Migration by zooplankton. *Limnology and Oceanography* **61**:
765–770. doi:[10.1002/lno.10251](https://doi.org/10.1002/lno.10251)

Ohman, M. D., J. A. Runge, E. G. Durbin, D. B. Field, and B. Niehoff. 2002. On birth and
death in the sea. *Hydrobiologia* **480**: 55–68. doi:[10.1023/A:1021228900786](https://doi.org/10.1023/A:1021228900786)

Pan, J., F. Cheng, and F. Yu. 2018. [The diel vertical migration of zooplankton in the hypoxia
area observed by video plankton recorder](#). *IJMS* Vol.47(07) [July 2018].

PEARRE Jr., S. 2003. Eat and run? The hunger/satiation hypothesis in verti-
cal migration: history, evidence and consequences. *Biological Reviews* **78**: 1–79.
doi:[10.1017/S146479310200595X](https://doi.org/10.1017/S146479310200595X)

Picheral, M., C. Catalano, D. Brousseau, and others. 2022. The Underwater Vision Profiler 6:
an imaging sensor of particle size spectra and plankton, for autonomous and cabled plat-
forms. *Limnology and Oceanography: Methods* **20**: 115–129. doi:[10.1002/lom3.10475](https://doi.org/10.1002/lom3.10475)

Picheral, M., S. Colin, and J.-O. Irisson. [EcoTaxa, a tool for the taxonomic classification of
images](#).

Picheral, M., L. Guidi, L. Stemann, D. M. Karl, G. Iddaoud, and G. Gorsky. 2010. The
Underwater Vision Profiler 5: An advanced instrument for high spatial resolution studies of
particle size spectra and zooplankton. *Limnology and Oceanography: Methods* **8**: 462–473.
doi:[10.4319/lom.2010.8.462](https://doi.org/10.4319/lom.2010.8.462)

615 Pinti, J., T. Kiørboe, U. H. Thygesen, and A. W. Visser. 2019. Trophic interactions drive
 616 the emergence of diel vertical migration patterns: A game-theoretic model of copepod
 617 communities. *Proceedings of the Royal Society B: Biological Sciences* **286**: 20191645.
 618 doi:[10.1098/rspb.2019.1645](https://doi.org/10.1098/rspb.2019.1645)

619 Royle, J. A. 2006. Site Occupancy Models with Heterogeneous Detection Probabilities. *Bio-*
 620 *metrics* **62**: 97–102. doi:[10.1111/j.1541-0420.2005.00439.x](https://doi.org/10.1111/j.1541-0420.2005.00439.x)

621 Schnetzer, A., and D. K. Steinberg. 2002. Active transport of particulate organic carbon and
 622 nitrogen by vertically migrating zooplankton in the Sargasso Sea. *Marine Ecology Progress*
 623 *Series* **234**: 71–84. doi:[10.3354/meps234071](https://doi.org/10.3354/meps234071)

624 Siegel, D. A., T. DeVries, I. Cetinić, and K. M. Bisson. 2023. Quantifying the ocean’s biological
 625 pump and its carbon cycle impacts on global scales. *Annual Review of Marine Science* **15**:
 626 null. doi:[10.1146/annurev-marine-040722-115226](https://doi.org/10.1146/annurev-marine-040722-115226)

627 Sonnet, V., L. Guidi, C. B. Mouw, G. Puggioni, and S.-D. Ayata. 2022. Length, width, shape
 628 regularity, and chain structure: time series analysis of phytoplankton morphology from
 629 imagery. *Limnology and Oceanography* **67**: 1850–1864. doi:[10.1002/lno.12171](https://doi.org/10.1002/lno.12171)

630 Soviadan, Y. D., F. Benedetti, M. C. Brandão, and others. 2022. Patterns of mesozooplankton
 631 community composition and vertical fluxes in the global ocean. *Progress in Oceanography*
 632 **200**: 102717. doi:[10.1016/j.pocean.2021.102717](https://doi.org/10.1016/j.pocean.2021.102717)

633 Steinberg, D. K., C. A. Carlson, N. R. Bates, S. A. Goldthwait, L. P. Madin, and A. F. Michaels.
 634 2000. Zooplankton vertical migration and the active transport of dissolved organic and
 635 inorganic carbon in the Sargasso Sea. *Deep Sea Research Part I: Oceanographic Research*
 636 *Papers* **47**: 137–158. doi:[10.1016/S0967-0637\(99\)00052-7](https://doi.org/10.1016/S0967-0637(99)00052-7)

637 Steinberg, D. K., C. A. Carlson, N. R. Bates, R. J. Johnson, A. F. Michaels, and A. H.
 638 Knap. 2001. Overview of the US JGOFS Bermuda Atlantic Time-series Study (BATS):
 639 a decade-scale look at ocean biology and biogeochemistry. *Deep Sea Research Part II:*
 640 *Topical Studies in Oceanography* **48**: 1405–1447. doi:[10.1016/S0967-0645\(00\)00148-X](https://doi.org/10.1016/S0967-0645(00)00148-X)
 641 Steinberg, D. K., and M. R. Landry. 2017. Zooplankton and the ocean carbon cycle. *Annual*
 642 *Review of Marine Science* **9**: 413–444. doi:[10.1146/annurev-marine-010814-015924](https://doi.org/10.1146/annurev-marine-010814-015924)
 643 Trudnowska, E., L. Lacour, M. Ardyna, A. Rogge, J. O. Irisson, A. M. Waite, M. Babin, and
 644 L. Stemann. 2021. Marine snow morphology illuminates the evolution of phytoplankton
 645 blooms and determines their subsequent vertical export. *Nature Communications* **12**: 2816.
 646 doi:[10.1038/s41467-021-22994-4](https://doi.org/10.1038/s41467-021-22994-4)
 647 Turner, J. 2004. The importance of small planktonic copepods and their roles in pelagic marine
 648 food webs,.
 649 Vilgrain, L., F. Maps, M. Picheral, M. Babin, C. Aubry, J.-O. Irisson, and S.-D. Ayata.
 650 2021. Trait-based approach using in situ copepod images reveals contrasting ecological
 651 patterns across an Arctic ice melt zone. *Limnology and Oceanography* **66**: 1155–1167.
 652 doi:[10.1002/lno.11672](https://doi.org/10.1002/lno.11672)
 653 Whitmore, B. M., and M. D. Ohman. 2021. Zooglider-measured association of zooplank-
 654 ton with the fine-scale vertical prey field. *Limnology and Oceanography* **66**: 3811–3827.
 655 doi:[10.1002/lno.11920](https://doi.org/10.1002/lno.11920)